https://doi.org/10.5194/acp-2022-566
Preprint. Discussion started: 15 August 2022

Atmospheric Chemistry and Physics Discussions
Open Access

Product distribution, kinetics, and aerosol formation from the OH oxidation of dimethyl sulfide under different RO_2 regimes

Qing Ye[1*], Matthew B. Goss[1], Jordan E. Krechmer[2], Francesca Majluf[2], Alexander Zaytsev[3], Yaowei Li[3], Joseph R. Roscioli[4], Manjula Canagaratna[2], Frank N. Keutsch[3,5], Colette L. Heald[1] and Jesse H. Kroll[1]

[1]Department of Civil and Environmental Engineering, Massachusetts Institute of Technology, Cambridge, Massachusetts 02139, United States

[2]Center for Aerosol and Cloud Chemistry, Aerodyne Research Incorporated, Billerica, Massachusetts 01821, United States

[3]John A. Paulson School of Engineering and Applied Sciences, Harvard University, Cambridge, Massachusetts 02138, United States

[4]Center for Atmospheric and Environmental Chemistry, Aerodyne Research Incorporated, Billerica, Massachusetts 01821, United States

[5]Department of Chemistry and Chemical Biology, Department of Earth and Planetary Sciences, Harvard University, Cambridge, Massachusetts 02138, United States

[*]Now at the Atmospheric Chemistry Observations and Modeling Laboratory, National Center for Atmospheric Research, Boulder, Colorado 80301, United States

Correspondence to: Qing Ye (qingye@ucar.edu), Jesse H. Kroll (jhkroll@mit.edu)

Abstract. The atmospheric oxidation of dimethyl sulfide (DMS) represents a major natural source of atmospheric sulfate aerosols. However, there remain large uncertainties in our understanding of the underlying chemistry that governs the product distribution and sulfate yield from DMS oxidation. Here, chamber experiments were conducted to simulate gas-phase OH-initiated oxidation of DMS under a range of reaction conditions. Most importantly, the bimolecular lifetime (τ_{bi}) of the peroxy radical CH_3SCH_2OO was varied over several orders of magnitude, enabling the examination of the role of peroxy radical isomerization reactions on product formation. An array of analytical instruments was used to measure nearly all sulfur-containing species in the reaction mixture, and results were compared with a near-explicit chemical mechanism. When relative humidity was low, "sulfur closure" was achieved under both high-NO ($\tau_{bi} < 0.1$ s) and low-NO ($\tau_{bi} > 10$ s) conditions, though product distributions were substantially different in the two cases. Under high-NO conditions, approximately half the product sulfur was in the particle phase, as methane sulfonic acid (MSA) and sulfate, with most of the remainder as SO_2 (which in the atmosphere would eventually oxidize to sulfate or be lost to deposition). Under low-NO conditions, hydroperoxymethyl thioformate (HPMTF, $HOOCH_2SCHO$), formed from CH_3SCH_2OO isomerization, dominates the sulfur budget over the course of the experiment, suppressing or delaying the formation of SO_2 and particulate matter. The isomerization rate constant of CH_3SCH_2OO at 295 K is found to be 0.13 ± 0.03 s^{-1}, in broad agreement with other recent laboratory measurements. The rate constants for the OH oxidation of key first-generation oxidation products (HPMTF and methyl thioformate, MTF) were also determined ($k_{OH+HPMTF} = 2.1 \times 10^{-11}$ cm^3 $molec^{-1}$ s^{-1}, k_{OH+MTF} 1.35×10^{-11} cm^3 $molec^{-1}$ s^{-1}). Product measurements agree reasonably well with mechanistic predictions in terms of total sulfur distribution and concentrations of most individual species,

https://doi.org/10.5194/acp-2022-566
Preprint. Discussion started: 15 August 2022

though the mechanism overpredicts sulfate and underpredicts MSA under high-NO conditions. Lastly, results from high-RH conditions suggest efficient heterogenous loss of at least some gas-phase products.

1 Introduction

Dimethyl sulfide (DMS), emitted by marine phytoplankton, is an important natural source of sulfur to the atmosphere (Kloster et al., 2006; Lana et al., 2011). The atmospheric oxidation of DMS represents a dominant source of non-sea salt sulfate aerosols, and as such can play an important role in global aerosol climate effects (Charlson et al., 1987; Rap et al., 2013). The chemistry by which DMS oxidizes to form sulfate is highly complex: the mechanism includes multiple branch points and intermediate species, and many reaction rates and product yields are uncertain and/or highly dependent on reaction conditions (Barnes et al., 2006; Hoffmann et al., 2016). As a result, many large-scale models adopt a highly simplified DMS chemistry with fixed SO_2 yields, usually without inclusion of other intermediates (Chin et al., 1996; Huijnen et al., 2010; Kloster et al., 2006; Lamarque et al., 2012). Such a simplified approach may lead to errors in predicted aerosol radiative effects, in the past, present, and future atmospheres (Fung et al. 2021).

The major daytime sink of DMS is its reaction with OH radicals. The detailed DMS + OH reaction scheme is shown in Figure 1. A key branch point in DMS + OH is the methylthiomethylperoxy radical (CH_3SCH_2OO) formed from H-atom abstraction followed by O_2 addition. The subsequent chemistry of this radical plays a determining role in the overall product distribution, and thus likely influences the amount of sulfate aerosols that are ultimately formed. As with all large RO_2 species, CH_3SCH_2OO radicals may undergo bimolecular reactions (with NO and HO_2) or unimolecular reaction via a recently-identified (Berndt et al., 2019; Veres et al., 2020; Wu et al., 2015; Ye et al., 2021) isomerization channel:

$$CH_3SCH_2OO + NO \rightarrow CH_3SCH_2O + NO_2 \quad (1)$$

$$CH_3SCH_2OO + HO_2 \rightarrow CH_3SCH_2OOH + O_2 \quad (2)$$

$$CH_3SCH_2OO \rightarrow CH_2SCH_2OOH \quad (3)$$

CH_3SCH_2OO may also react with other RO_2 radicals (Barnes et al., 2006), though this process is likely to be minor under atmospheric conditions. The CH_3SCH_2O radical formed from the NO pathway (Reaction 1) is believed to rapidly form SO_2, sulfate, and methanesulfonic acid (MSA) (Barnes et al., 2006). The alkyl radical derived from Reaction 3 will react with O_2 to form $OOCH_2SCH_2OOH$, which will undergo a second isomerization reaction to form hydroperoxymethyl thioformate (HPMTF, $HOOCH_2SCHO$), as shown in Figure 1.

The branching fraction of the CH_3SCH_2OO radical depends on the concentrations of NO and HO_2 and the rate constants of Reactions 1-3. The rate constant for the isomerization reaction, k_{isom}, is particularly uncertain, as values determined in previous studies span a very wide range, from ~ 0.04 s^{-1} to ~2 s^{-1} near room temperature (Berndt et al., 2019; Veres et al., 2020; Wu et

https://doi.org/10.5194/acp-2022-566
Preprint. Discussion started: 15 August 2022

al., 2015; Ye et al., 2021). This highlights a major challenge in predicting CH_3SCH_2OO branching and the subsequent aerosol formation, both in the pristine atmosphere and in environments affected by anthropogenic emissions.

Most previous experimental studies investigating DMS oxidation have examined individual products and reaction steps in isolation (Barnes et al., 2006; Berndt et al., 2019; Jernigan et al., 2022; Mihalopoulos et al., 1992; Patroescu et al., 1996); very few studies of the entire multiphase and multistep reaction system have been conducted, especially under conditions in which the recently-discovered isomerization pathway (Reaction 3) may compete. Therefore, there exist few studies that can test our overall understanding of the reaction system, by comparison against predictions by state-of-the-art reaction mechanisms. Recently, we conducted laboratory measurements of a broad suite of organic sulfur products and sulfate aerosols from DMS + OH, and estimated k_{isom} to be 0.09 s^{-1} (0.03 – 0.3 s^{-1}, $1\sigma_g$) (Ye et al., 2021); however this was for a single reaction condition only (low RH, ~ 1 ppb NO), and SO_2 (a major inorganic sulfur-containing product) was not measured.

Here we extend our previous work by conducting a series of chamber experiments of DMS + OH under a wide range of values of the CH_3SCH_2OO bimolecular lifetime (τ_{bi}), and comprehensively characterizing sulfur-containing products (organic and inorganic, gas-phase and particulate), with the aim of accounting for all (or nearly all) reacted sulfur. Such "sulfur closure" measurements enable direct comparisons with predictions from a mechanistic model, in order to assess our current mechanistic understanding and identify possible gaps in this understanding. These measurements also enable the determination of key kinetic parameters in the reaction systems. In one experiment, we vary τ_{bi} over a wide range to estimate the k_{isom} of the CH_3SCH_2OO radical, obtaining a k_{isom} with a much smaller uncertainty range than in our previous study. The rate constants for the OH oxidation of key first-generation oxidation products (HPMTF and methyl thioformate, MTF) are also deterimined. Lastly, we investigate the effect of relative humidity on the DMS+OH product distributions.

2. Method and Materials

Experiments were conducted in a 7.5 m^3 temperature-controlled environmental chamber, held at 295 K (Hunter et al., 2014). The chamber is surrounded by 48 ultraviolet lights (Q-Lab) with a peak irradiance at 340 nm. Before each experiment, the chamber was flushed by zero air (Aadco, 737 series) for at least 12 hours to ensure a clean gas and particle background. Throughout the course of each experiment, a constant flow of zero air was introduced into the chamber to replenish the flow drawn by the instruments. For high-RH experiments, the replenishment flow was first sent through a bubbler filled with Milli-Q water before entering the chamber. The rate of chamber dilution was derived by measuring the decay of acetonitrile, injected at low concentrations (5 ppb) in the beginning of each experiment. The overall dilution lifetime was approximately 10 hours. Concentrations of all species reported below have been corrected for dilution.

The evolving chemical composition of the reaction mixture was monitored by a suite of real-time instruments located outside the chamber. The Supplementary Information provides instrument details, as well as the sulfur species detected by each (Table

Atmospheric Chemistry and Physics Discussions

S1). Briefly, DMS and lightly oxygenated gaseous species were measured by a Vocus proton-transfer-reaction time-of-flight mass spectrometer (Vocus-PTR-MS, Aerodyne Research Inc.) (Krechmer et al., 2018). More oxygenated gaseous species were measured by an iodide time-of-flight chemical ionization mass spectrometer (I^--CIMS, Aerodyne Research Inc.) (Lee et al., 2014) and an ammonium time-of-flight chemical ionization mass spectrometer (NH_4^+-CIMS, Ionicon Analytik) (Zaytsev et al., 2019). SO_2 was detected by a compact tunable infrared laser direct absorption spectrometer (TILDAS, Aerodyne Research Inc.) (McManus et al., 2011; McManus et al., 1995). Particle-phase products, namely sulfate and MSA, were measured by an aerosol mass spectrometer (AMS, Aerodyne Research Inc.) (DeCarlo et al., 2006). The quantification of MSA was determined from the AMS tracer ion $CH_3SO_2^+$ (see SI); this ion is unique to MSA/methylsulfonate, with negligible contributions from other sulfur-containing species (Hodshire et al., 2019; Huang et al., 2015). Our multi-instrument approach enables the measurement of essentially all closed-shelled sulfur products known in the DMS oxidation mechanism, except for OCS, which accounts for a very small (less than a couple percent) sulfur yield from DMS oxidation (Barnes et al., 1994; Jernigan et al., 2022). Complementary instruments include an ozone monitor (2B Tech), a NO-NO_2-NO_x Analyzer (Thermo Scientific), a scanning mobility particle sizer (TSI), and a temperature and RH sensor (TE Connectivity). More details of the instruments, including their calibrations and measurement uncertainties, are provided in the Supporting Information.

The experiments carried out in this study are listed in Table 1. At the beginning of each experiment, DMS, the acetonitrile dilution tracer, seed particles, and the OH precursor were added to the chamber and allowed to become well mixed. Seed particles (ammonium nitrate, sodium nitrate, or sodium chloride), were added via atomization, providing surface area for condensing vapors. Particle condensation timescales (seconds to 10's of seconds) were much shorter than the condensation timescale of low-volatility species onto the chamber wall (~ 2000 s, as determined previously for this chamber (Zaystev et al, 2019)). DMS was introduced by gently heating a known volume (1 – 2 uL) from a needle syringe and the vapor was carried into the chamber by the dilution flow. For the high τ_{bi} experiments, in which HPMTF formation was expected (see Table 1), DMS-$^{13}C_2$ (99 atom % ^{13}C, Millipore Sigma) was added as the precursor in addition to unlabeled DMS (>99%, Millipore Sigma), in order to separate HPMTF ($C_2H_4SO_3{\bullet}I^-$, *m/z* 234.893) from N_2O_5 ($N_2O_5{\bullet}I^-$, *m/z* 234.886) in the I^--CIMS. The use of DMS-$^{13}C_2$ is expected to have little effect on the observed reaction kinetics in this study. For the high-NO (low τ_{bi}) experiments, HONO (10's of ppb) was added as the OH precursor, by passing air over a mixture of sodium nitrite and sulfuric acid and into the chamber. For low-NO (high τ_{bi}) experiments, ~ 3 ppm of H_2O_2 was added as the OH precursor, by vaporizing a known amount of 30% H_2O_2 solution. In some experiments (Exp. 2b, 3, and 5), aliquots of HONO or NO were added in the middle of the experiment to change reaction conditions. After all reagents were well-mixed (> 5 mins), the UV lights were turned on to photolyze HONO and/or H_2O_2, generating OH radicals and initiating reaction. The OH concentration was estimated from the decay of DMS (using $k_{OH+DMS} = 6.97 \times 10^{-12}$ cm^3 molec^{-1} s^{-1}) (Jenkin et al., 1997; Saunders et al., 2003), and was used to determine the equivalent atmospheric OH exposure time assuming $[OH]_{atm} = 1.5 \times 10^6$ molec cm^{-3}.

A 0-D model (the Framework for 0-D Atmospheric Modeling, F0AM) (Wolfe et al., 2016) coupled with the Master Chemical Mechanism (MCMv3.3.1) (Jenkin et al., 1997; Saunders et al., 2003) was used to simulate gas-phase DMS oxidation in each experiment. Here, the DMS scheme in the MCM was updated primarily based on Wu *et al.* (Wu et al., 2015) with the isomerization rate constant of the CH_3SCH_2OO radical as 0.09 s^{-1}, taken from our previous work (Ye et al., 2021). The complete reaction scheme is shown in Figure 1. Newly-added reactions with rate constants beyond the original MCM scheme are listed in Table S1. Model inputs, including concentrations of the precursor, oxidant, and chamber conditions including temperature, light intensity, and dilution rate were taken directly from the measurements. The model describes gas-phase chemistry only, and so phase partitioning and heterogeneous chemistry is not described; instead, all sulfuric acid and MSA formed is assumed to instantaneously partition to the particle phase. In the high-NO experiments, model NO concentrations were constrained to values measured by the NO-NO_2-NO_x analyzer. In the low-NO experiment (Exp. 2a) in which the sub-ppb-level NO concentration was below the detection limit of the NO_x analyzer, the model was used to constrain background NO concentration by matching the modeled DMS decay to the measured decay (Ye et al., 2021). The estimated [NO] in Exp. 2a is ~ 10 ppt.

3. Results and discussions

3.1 Comprehensive measurements of S-containing products

Figure 2a-b show the measured product evolution from Experiments 1 and 2a. A range of sulfur-containing products were measured in both the gas and aerosol phases, shown as stacked colored traces. All concentrations are given in parts-per-billion sulfur (ppb S), and are presented as a function of atmosphere-equivalent OH exposure time. Shown in grey is the amount of DMS oxidized over the course of the experiment. By the end of the experiment, only a fraction of the DMS had been consumed, since OH exposures were not high enough to fully deplete the DMS. In Exp. 1 (high-NO, Figure 2a), HONO was used as the OH precursor, and the NO was kept at ~50 ppb by continuous addition, ensuring that the dominant fate of the RO_2 radicals was reaction with NO (τ_{bi} < 0.1 s). After ~12 hr of atmosphere-equivalent OH exposure, 104% (100% - 124%, 1σ) of the reacted sulfur was measured as products, indicating excellent sulfur closure. The uncertainty in sulfur closure includes uncertainty in both gas-phase and particle-phase measurements (see SI for more details). Major sulfur-containing products were SO_2, particulate MSA, and particulate sulfate, with 48% of the product sulfur found in the particle phase. Minor species observed included dimethyl sulfoxide (DMSO), $C_2H_6SO_2$ (likely dimethyl sulfone, $DMSO_2$) and methane sulfinic acid (MSIA), known products from the addition channel, and CH_2SO_2 (a sulfene or thioacid) and CH_3SO_6N (likely methanesulfonyl peroxynitrate). No HPMTF was observed in these experiments, which is expected given the short bimolecular RO_2 lifetime.

In Exp. 2a (low-NO, Fig 1b), H_2O_2 was the OH precursor, and NO and HO_2 levels were sufficiently low (~10 ppt and 100 ppt, respectively) that RO_2 isomerization dominated (τ_{bi} > 10 s). Product distributions are dramatically different than those under high-NO conditions. The total sulfur products measured accounted for nearly all, 90% (64% - 118%) of the reacted DMS sulfur; this sulfur closure is good but slightly worse than in Exp. 1. The larger uncertainty range is due to the uncertainty of the HPMTF calibration in the I^--CIMS. However, the near sulfur closure, combined with the HPMTF yields (discussed in Section 3.3) suggest that our estimated sensitivity is reasonably accurate, and thus our overall uncertainty of total sulfur may be an overestimate.

Due to the long RO_2 bimolecular lifetime ($\tau_{bi} > 10$ s), the dominant product is HPMTF from CH_3SCH_2OO isomerization; this accounts for about half of the reacted sulfur (60% of the measured product sulfur). It is expected that a negligible amount (1 % or less) of HPMTF was lost to the chamber wall under the experimental condition here based on its estimated vapor pressure (see SI). The time series of $C_2H_4SO_3$-$^{12}C_2$ in the I^--CIMS ($C_2H_4SO_3{\bullet}I^-$) and the NH_4^+-CIMS ($C_2H_4SO_3{\bullet}NH_4^+$), shown in Figure S2, match very well. This indicates that (1) NH_4^+-CIMS is able to detect HPMTF (which to our knowledge has not been demonstrated previously) and (2) there was negligible N_2O_5 formation from the residual NO_x in the chamber, since N_2O_5 is not measurable by the NH_4^+-CIMS, and therefore our quantification of HPTMF-$^{12}C_2$ in Exp. 2a with I^--CIMS is free of N_2O_5 interferences. Only 3.3% (3.1% - 5.4%) of the reacted sulfur was found in the aerosol in the low-NO experiment after ~6 h of OH exposure.

3.2 Measurement-model comparison

The (near) sulfur closure of the experiments, in which virtually all the reacted sulfur was measured as products, enables a comparison with the mechanistic model. MCM predictions for the two experiments described above (Exp. 1 and 2a) are shown in Figure 2c-d; individual species are also compared in Figures S4 and S5. Under high-NO conditions, measurements and model predictions (Figures 2a and 2c, Figure S3) agree well for gas-phase species and for total particulate sulfur. However, the two differ greatly in terms of particle-phase composition: AMS measurements indicate ~70% of the particle-phase sulfur is MSA, with the remainder sulfate; by contrast, the model predicts that sulfate dominates, with negligible contribution from MSA. This suggests the mechanism may underestimate the rate of MSA formation, and/or estimate the rate of sulfuric acid formation.

In the model, both MSA and sulfuric acid are formed from reactions of the $CH_3S(O)_2O$ radical:

$$CH_3S(O)_2O + HO_2 \rightarrow CH_3S(O)_2OH\ (MSA) + O_2 \quad (4)$$

$$CH_3S(O)_2O + M \rightarrow CH_3 + SO_3 \quad (5)$$

Reaction 5 generates sulfur trioxide (SO_3), which will quickly hydrolyze to form sulfuric acid. SO_3 can also be formed by the OH oxidation of SO_2, but this reaction would occur over 50 h of OH exposure, much longer than the oxidation timescale in Exp 1. Since the measured and modeled total particulate sulfur (MSA + sulfate) agree well, the model-measurement differences in the ratio of MSA to sulfuric acid likely relate to the relative rates of these $CH_3S(O)_2O$ reactions. It is possible that the rate constant of Reaction 4 is underestimated in the mechanisms, but if it is increased it to a gas-kinetic rate (3×10^{-10} cm^3 molec^{-1} s^{-1}), MSA is still not predicted to dominate over sulfuric acid. Instead, the decomposition of $CH_3S(O)_2O$ (Reaction 5), which has received little study, might be slower than the value used in the mechanism (~0.09 s^{-1}), leading to slower sulfuric acid formation. Alternatively, MSA might be formed by the reaction of $CH_3S(O)_2O$ with species other than HO_2, such as DMS or HCHO (Barnes et al., 2006; Yin et al., 1990). While such reactions are unlikely to be important in the atmosphere, they might occur in laboratory experiments, which have relatively high concentrations of organic species. However, the kinetics of such reactions are not well known, and warrant future research.

In the low-NO case (Figures 2b and 2d, Figure S4), measured and modeled concentrations also broadly agree. The predicted concentration of HPMTF is lower (by ~ 30%) than what was measured. This could be due to the uncertainty in the sensitivity of HPMTF in the I^--CIMS, and/or in the k_{isom} value used in the model. The k_{isom} value used, 0.09 s^{-1}, is derived from our previous study (Ye et al., 2021); as discussed below, this value agrees with that determined in this work. Compared to measurements, the model also predicts somewhat higher concentrations of minor sulfur-containing products, such as DMSO, $C_2H_6SO_2$ ($DMSO_2$ + CH_3SCH_2OOH), MSIA, and MTF. This could be caused by overestimates of instruments' sensitivities, uncertainties in the rate constants in the model, or some losses to surfaces. Nevertheless, overall the model and measurements agree quite well, with product formation dominated by HPMTF, and little aerosol formation since low-volatility species (MSA and sulfuric acid) can only be formed as later-generation products.

3.3 Determination of k_{isom}

The fate of the CH_3SCH_2OO radical, and hence the product distribution of DMS oxidation, relies critically on the isomerization rate constant of the CH_3SCH_2OO radical (k_{isom}). In our previous work we determined k_{isom} from a single reaction condition (at one value of τ_{bi}), and the value had a large uncertainty due to the poorly-constrained sensitivity of HPMTF in the CIMS. Here, we determine k_{isom} by examining product formation at multiple values of τ_{bi}, similar to previous measurements of isomerization rates of terpene-derived RO_2 radicals (Xu et al., 2019). HONO or NO was added to the chamber several times during the experiment (Figure S6), perturbing the branching of the CH_3SCH_2OO radical (isomerization vs bimolecular reactions). The total S measurements are shown in Figure S8.

The yield of HPMTF in the abstraction channel (Δ[HPMTF]/(Δ$[DMS]_{abs}$) was calculated for each perturbation as a function of τ_{bi} after taking into the account of loss via OH oxidation ($k_{OH+HPMTF}$ = 2.1 × 10^{-11} cm^3 $molec^{-1}$ s^{-1}, see Section 3.4). The detailed calculation is described in the Supplementary Information (Eq. S1 – Eq. S4). Figure 3a shows the HPMTF yield as a function of τ_{bi}. As expected, the yield increases dramatically with τ_{bi}, and fitting this data to Equation S4 (given in the SI) enables the determination of k_{isom}. The best-fit value for k_{isom} is 0.13 ± 0.03 s^{-1}. The uncertainty is much smaller than in our previous determination (Ye et al., 2021) since the fit depends only on the shape (the inflection point) of the curve and not the absolute yield values, and thus is insensitive to the uncertain HPTMF calibration factor. Nonetheless, since the asymptotic (high τ_{bi}) value is close to 1 (1.5), our estimated calibration factor appears to be reasonably accurate.

https://doi.org/10.5194/acp-2022-566
Preprint. Discussion started: 15 August 2022

The three data points with higher HPMTF yields (top of Fig 3a) were collected in the latter half of the experiment, after HPMTF had built up in the chamber, and therefore correcting for OH loss resulted in an increased HPMTF yield. Because of their larger measurement uncertainties, these data points have smaller effects on the overall fit to Equation S4. If the OH loss is not included, k_{isom} = 0.11 ± 0.02 s^{-1} (Equation S4 and Figure S7).

Figure 3b compares our value of k_{isom} with previous measurements and theoretical determinations (T=293-298 K) (Berndt et al., 2019; Jernigan et al., 2022; Veres et al., 2020; Wu et al., 2015; Ye et al., 2021). Our measured value of k_{isom} is consistent with our previous (single τ_{bi}) measurement (Ye *et al*., 2021) though with a much reduced uncertainty, and is also in broad agreement with measured values from Berndt *et al.* (0.23 ± 0.12 s^{-1}) and Jernigan *et al.* (0.1 ± 0.05 s^{-1}).

3.4 Reaction rates of OH with HPMTF and MTF

Here we examine the oxidation of HPMTF and MTF, two species whose chemical fates are not well known. Both were formed only under low-NO conditions (Exp. 2a); because of the relatively low OH concentrations of that experiment, their concentrations increased throughout the entire experiment, with no subsequent decay. Thus, to estimate $k_{OH+HPMTF}$ and k_{OH+MTF}, high concentrations of NO (~70 ppb) were introduced at the end of Experiment 2 (denoted as Exp. 2b, shown in Figure S5). The large amount of NO essentially terminated the production of HPMTF and MTF, and at the same time increased the OH concentration in the chamber. The loss of HPMTF during this period is expected to be dominated by OH reaction, because the high level of NO precluded substantial oxidation by O_3 and NO_3. Photolysis of HPMTF is also unlikely to contribute to the observed decay: by assuming that its photolytic cross sections are equal to the summed cross section of aldehydes and organic peroxides groups using rate constants in MCM (Khan et al., 2021), we estimate that photolysis accounted for only 4% of the HPMTF loss in our chamber.

The decay of HPMTF (Figure S5c), is consistent with a $k_{OH+HPMTF}$ of 2.1 (2.0 – 2.2) × 10^{-11} cm^3 $molec^{-1}$ s^{-1}. This is in agreement with recent measurements of Jernigan *et al*. (1.4 (0.27 – 2.4) × 10^{-11} cm^3 $molec^{-1}$ s^{-1}); both experimental values are an order of magnitude higher than an earlier theoretical estimate of the rate (1.2 × 10^{-12} cm^3 $molec^{-1}$ s^{-1}) (Wu et al., 2015). Using this lower value, Khan *et al*. estimated that photolysis loss dominates HPMTF sink in the global marine sulfur budget, with OH oxidation only accounting for 10% of HPMTF loss (Khan et al., 2021). This higher OH rate constant suggests that OH oxidation is in fact likely to be an important loss process for HPMTF, at least when liquid water is not present (Fung et al., 2021).

MTF is formed as a second-generation DMS oxidation product from CH_3SCH_2OOH + OH in low-NO conditions. Using a similar method as $k_{OH+HPMTF}$, the k_{OH+MTF} is estimated to be 1.35 (1.3 – 1.4) × 10^{-11} cm^3 $molec^{-1}$ s^{-1}, which agrees with the only other measurement of k_{OH+MTF}, 1.11 ± 0.22 × 10^{-11} cm^3 $molec^{-1}$ s^{-1}, by Patroescu *et al* (Patroescu et al., 1996).

3.5 Role of relative humidity

The experiments described above were carried out under dry conditions and thus focus only on homogenous gas-phase chemistry; heterogeneous and aqueous-phase processes may also be important contributors to DMS oxidation chemistry (Hoffmann et al., 2016). Thus, Experiments 4 and 5 were carried out at 65% RH, under high- and low-NO levels, respectively. These experiments were carried out over longer timescales (higher OH exposures) than the corresponding dry experiments.

Results from Exp. 4 (in which 50 - 100 ppb NO was maintained in the chamber) are shown in Figure 4a. The overall product distribution is similar to that under dry conditions (Figure 2a), with SO_2, MSA, and sulfate being the major reaction products. The modeled product distribution shown in Figure S9 (a) is largely the same as that in the dry experiment (Figure 2c), as water does not play a role in the gas-phase oxidation mechanism shown in Figure 1. Even though this experiment was carried out over longer timescales, the measured sulfur closure is quite good, 107% (99% - 171%) of the reacted DMS at the end of the experiment. Figure 4c compares the evolving concentrations of major product species under high- and low-RH conditions, presented as change in product concentration relative to change in DMS concentration, over the initial OH exposure (corresponding to that of Exp. 1). Over these timescales, species such as DMSO, SO_2 and MSA showed a relatively small effect of RH. By contrast, almost no $C_2H_6SO_2$ (likely $DMSO_2$) was measured in the gas phase under high RH. Within the time scale of the experiments, our measurements do not suggest conversion of MSA to sulfate in the aerosol phase, as predicted in some modeling studies (Fung et al., 2021, Chen et al., 2018). This difference may arise from low particle-phase OH concentrations in our experiments.

Figure 4b shows products from Exp. 5 (65% RH, low NO, $\tau_{bi} > 1$ s). As in the low-RH, high-τ_{bi} case (Exp. 2a, Figure 2b), HPMTF and SO_2 are the dominant measured products, and little aerosol formation is observed. One minor new product, with formula SO_6, was detected in the I^--CIMS in this experiment; it is likely an adduct or a fragment formed in the instrument, but the parent species is unknown. In contrast to the high-NO experiment (Exp. 4), sulfur closure was markedly worse than under dry conditions. In the first 6 hours of equivalent OH exposure (the timescale of the dry experiment), only 74% (53% - 97%) of the reacted sulfur was detected as products. This sulfur closure degraded still further as the experiment proceeded, and was only 23% (18% - 31%) at the end of the experiment. Here, I^--CIMS sensitivities derived from the dry calibration were used for species quantification, and therefore may underestimate the concentration under high RH (Lee et al., 2014). However, these differences would have to be dramatic (by factor of five or more) to account for all the reacted sulfur, and therefore such calibration errors are unlikely to explain the decreased sulfur closure.

Figure 4d shows differences for key product species formed in the high-τ_{bi} experiments under the high- and low-RH conditions, again over the timescales of the dry experiment. The initial yields of DMSO, $C_2H_6SO_2$, and HPMTF are not substantially different. SO_2 concentrations were lower under humid conditions, but with an absolute difference of only ~2 ppb. Thus the

https://doi.org/10.5194/acp-2022-566
Preprint. Discussion started: 15 August 2022

production rates of these species are not affected dramatically by RH level. Instead the poor sulfur closure at high RH suggests extra losses, most likely losses to surfaces. The low aerosol concentration towards the end of the experiment (due to particle wall loss over the long experimental time, ~ 17 h) could lead to substantial chamber wall loss of low-volatility products, which would contribute to this gap in measured sulfur. Such surface losses are likely exacerbated at high RH, due to uptake into the aqueous phase. The initial aerosol liquid water content (LWC) in the high-RH experiment was 10 – 100 μg m^3, orders of magnitude lower than LWC in maritime clouds (Wallace and Hobbs, 2006). Therefore, such losses may play an even more important role in the real atmosphere. Indeed, studies have suggested that uptake to cloud water may be an important sink of gas-phase HPMTF. Using airborne measurements, Novak *et al*. have shown that HPMTF is lost to clouds effectively and irreversibly in the marine boundary layer (Novak et al., 2021). Similarly, using a global model, Fung *et al*. found that including cloud uptake into a global model substantially decreases the global burden of HPMTF, by up to 86% (Fung et al., 2021).

3.5 Conclusions

In this study, we conducted a series of chamber experiments to investigate the total product distribution from DMS oxidation at different RO_2 fates and relative humidities. Under dry conditions, good sulfur closure was obtained, suggesting most of the sulfur-containing product species were accounted for. Under high-NO conditions (τ_{bi} < 0.1 s), major products are SO_2, MSA, and sulfate, whereas under low-NO condition (τ_{bi} > 10 s), HPMTF formed from RO_2 isomerization makes up about half of the product sulfur, with very little MSA or sulfate formation. Comparisons between measurements and MCM predictions show relatively good agreement for most species and total aerosol formation. However, under high-NO conditions, the model predicts much more sulfate and less MSA than was measured; this might indicate errors in the kinetics of the reactions that lead to rapid (first-generation) MSA or sulfate formation. This work also provides new measurements of the rate constants (at 295 K) of key reactions in the DMS oxidation mechanism, including k_{isom} (0.13 ± 0.03 s^{-1}), $k_{HPMTF+OH}$ (2.1 × 10^{-11} cm^3 $molec^{-1}$ s^{-1}) and k_{MTF+OH} (1.35 × 10^{-11} cm^3 $molec^{-1}$ s^{-1}). Our measured value of $k_{HPTMF+OH}$, which is consistent with that of Jernigan *et al*., suggests that OH is a more important gas-phase sink of HPTMF than photolysis. Lastly, results from high-RH conditions suggest heterogeneous losses of at least some of the products, indicating that uptake into the atmospheric aqueous phase (e.g., cloud droplets) may be an important sink as well.

Taken together, our results show that RO_2 fate has a controlling influence on the distribution of sulfur-containing products from DMS oxidation. In particular, the formation of HPMTF from RO_2 isomerization suppresses (or at least delays) the formation of SO_2, sulfate, and MSA. Additional studies are needed to constrain the temperature-dependence of k_{isom} to predict the formation of HPMTF (and other products) in warmer or colder environments, as well as to characterize the full multiphase product distribution under higher-RH conditions. In addition, experiments carried out over longer oxidation timescales, and with different oxidants, are needed to better understand the amount and rate of aerosol formation over days of oxidation. A related need is improved constraints on the atmospheric fate of HPMTF and other key reaction intermediates (e.g., DMSO, MSIA), including rates and products of gas-phase oxidation, aqueous-phase oxidation, and photolysis, as well as rates of physical loss (deposition and uptake).

Data availability

Chamber data and species concentrations for all experiments are publicly available via the Kroll group publication website http://krollgroup.mit.edu/publications.html.

Author contributions

QY, MBG, JEK, FM, AZ, YL, JRR collected the data. QY and MBG analyzed the data. MBG performed box model simulations. QY and JHK wrote the manuscript. MC, FNK, CLH and JHK provided project guidance. All authors were involved in helpful discussion and contributed to the manuscript.

Declaration

The authors declare that they have no conflict of interest.

Acknowledgements

This work was supported by the U.S. Department of Energy Office of Biological and Environmental Research under grant DE-SC0018934 and the Harvard Global Institute. The authors thank Timothy Bertram, Gordon Novak and Chris Jernigan at the University of Wisconsin-Madison for insightful discussions.

References

Barnes, I., Becker, K. H. and Patroescu, I.: The tropospheric oxidation of dimethy sulfide: a new source of carbonyl sulfide, Geophys. Res. Lett., 21(22), 2389–2392, 1994.

Barnes, I., Hjorth, J. and Mihalapoulos, N.: Dimethyl sulfide and dimethyl sulfoxide and their oxidation in the atmosphere, Chem. Rev., 106(3), 940–975, doi:10.1021/cr020529+, 2006.

Berndt, T., Scholz, W., Mentler, B., Fischer, L., Hoffmann, E. H., Tilgner, A., Hyttinen, N., Prisle, N. L., Hansel, A. and Herrmann, H.: Fast Peroxy Radical Isomerization and OH Recycling in the Reaction of OH Radicals with Dimethyl Sulfide, J. Phys. Chem. Lett., 10(21), 6478–6483, doi:10.1021/acs.jpclett.9b02567, 2019.

Charlson, R. J., Lovelock, J. E., Andreae, M. O. and Warren, S. G.: Oceanic phytoplankton, atmospheric sulphur, cloud albedo and climate, Nature, 326, 665–661, 1987.

Chen, Q., Sherwen, T. Evans, M. and Alexander, B.: DMS oxidation and sulfur aerosol formation in the marine troposphere: a focus on reactive halogen and multiphase chemistry, Atmos. Chem. Phys.,18, 13617–13637, doi:10.5184/acp-18-13617-2018, 2018.

Chin, M., Jacob, D. J., Gardner, G. M., Foreman-fowler, M. S., Spiro, P. A. and Savoie, D. L.: A global three-dimensional model of tropospheric sulfate, J. Geophys. Res., 101(D13), 18667–18690 [online] Available from: http://www.agu.org/journals/jd/v101/iD13/96JD01221/, 1996.

Decarlo, P. F., Kimmel, J. R., Trimborn, A., Northway, M. J., Jayne, J. T., Aiken, A. C., Gonin, M., Fuhrer, K., Horvath, T., Docherty, K. S., Worsnop, D. R. and Jimenez, J. L.: Aerosol Mass Spectrometer, Anal. Chem., 78(24), 8281–8289, doi:8410.1029/2001JD001213.Analytical, 2006.

Fung, K. M., Heald, C. L., Kroll, J. H., Wang, S., Jo, D. S., Gettlelman, A., Lu, Z., Liu, X., Zaveri, R. A., Apel, E., Blake, D. R., Jimenez, J.-L., Campuzano-Jost, P., Veres, P. R., Bates, T. S., Shilling, J. E. and Zawadowicz, M. A.: Exploring dimethyl sulfide (DMS) oxidation and implications for global aerosol radiative forcing, Atmos. Chem. Phys., 22(2), 1549–1573, doi:10.5194/acp-22-1549-2022, 2022.

Hodshire, A. L., Campuzano-Jost, P., Kodros, J. K., Croft, B., Nault, B. A., Schroder, J. C., Jimenez, J. L. and Pierce, J. R.: The potential role of methanesulfonic acid (MSA) in aerosol formation and growth and the associated radiative forcings, Atmos. Chem. Phys., 19(5), 3137–3160, doi:10.5194/acp-19-3137-2019, 2019.

Hoffmann, E. H., Tilgner, A., Schrödner, R., Bräuer, P., Wolke, R. and Herrmann, H.: An advanced modeling study on the impacts and atmospheric implications of multiphase dimethyl sulfide chemistry, Proc. Natl. Acad. Sci. U. S. A., 113(42), 11776–11781, doi:10.1073/pnas.1606320113, 2016.

Huang, D. D., Li, Y. J., Lee, B. P. and Chan, C. K.: Analysis of Organic Sulfur Compounds in Atmospheric Aerosols at the HKUST Supersite in Hong Kong Using HR-ToF-AMS, Environ. Sci. Technol., 49(6), 3672–3679, doi:10.1021/es5056269, 2015.

Huijnen, V., Williams, J., van Weele, M., van Noije, T., Krol, M., Dentener, F., Segers, A., Houweling, S., Peters, W., de Laat, J., Boersma, F., Bergamaschi, P., van Velthoven, P., Le Sager, P., Eskes, H., Alkemade, F., Scheele, R., Nedelec, P. and Patz, H.-W.: The global chemistry transport model TM5: description and evaluation of the tropospheric chemistry version 3.0, Geosci. Model Dev., 3, 445–473, 2010.

Hunter, J. F., Carrasquillo, A. J., Daumit, K. E. and Kroll, J. H.: Secondary Organic Aerosol Formation from Acyclic, Monocyclic, and Polycyclic Alkanes, Environ. Sci. Technol., 48, 10227–10234, 2014.

Jenkin, M. E., Saunders, S. M. and Pilling, M. J.: The tropospheric degradation of volatile organic compounds: a protocol for mechanism development, Atmos. Environ., 31(1), 81–104, 1997.

Jernigan, C. M., Fite, C. H., Vereecken, L., Berkelhammer, M. B., Rollins, A. W., Rickly, P. S., Novelli, A., Taraborrelli, D., Holmes, C. D. and Bertram, T. H.: Efficient production of carbonyl sulfide in the low-NOx oxidation of dimethyl sulfide, Geophys. Res. Lett., 2022.

Khan, M. A. H., Bannan, T. J., Holland, R., Shallcross, D. E., Archibald, A. T., Matthews, E., Back, A., Allan, J., Coe, H., Artaxo, P. and Percival, C. J.: Impacts of Hydroperoxymethyl Thioformate on the Global Marine Sulfur Budget, ACS Earth Sp. Chem., 5(10), 2577–2586, 2021.

Kloster, S., Feichter, J., Maier-Reimer, E., Six, K. D., Stier, P. and Wetzel, P.: DMS cycle in the marine ocean-atmosphere system – a global model study, Biogeosciences, 3(1), 29–51, 2006.

Krechmer, E. J., Lopez-Hilfiker, F., Koss, A., Hutterli, M., Stoermer, C., Deming, B., Kimmel, J., Warneke, C., Holzinger, R., Jayne, J., Worsnop, D., Fuhrer, K., Gonin, M. and Gouw, J. De: Evaluation of a New Reagent-Ion Source and Focusing Ion–Molecule Reactor for Use in Proton-Transfer-Reaction Mass Spectrometry, Anal. Chem., 90, 12011–12018, doi:10.1021/acs.analchem.8b02641, 2018.

Lamarque, J.-F., Emmons, L. K., Hess, P. G., Kinnison, D. E., Tilmes, S., F., V., Heald, C. L., Holland, E. A., Lauritzen, P. H., J., N., Rasch, P. J. and Tyndall, G. K.: CAM-chem: description and evaluation of interactive atmospheric chemistry in the Community Earth System Model, Geosci. Model Dev., 5, 369–411, 2012.

Lana, A., Bell, T. G., Simo, R., Vallina, S. M., Ballabrera-Poy, J., Kettle, A. J., Dachs, J., Bopp, L., Saltzman, E. S., Stefels, J., Johnson, J. . E. and Liss, P. S.: An updated climatology of surface dimethlysulfide concentrationsand emission fluxes in the global ocean, Global Biogeochem. Cycles, 25, GB1004, 2011.

Lee, B. H., Lopez-Hilfiker, F. D., Mohr, C., Kurtén, T., Worsnop, D. R. and Thornton, J. A.: An iodide-adduct high-resolution time-of-flight chemical-ionization mass spectrometer: Application to atmospheric inorganic and organic compounds, Environ. Sci. Technol., 48(11), 6309–6317, doi:10.1021/es500362a, 2014.

McManus, J.B., Zahniser, M.S., Nelson, D.D., McGovern, R.M., Agnese, M. and Brown, W.F.: Compact Quantum Cascade Laser Instrument for High Precision Trace Gas Measurements. In Optical Instrumentation for Energy and Environmental Applications (p. EThC2). Optica Publishing Group, 2011, November.

McManus, J.B., Kebabian, P.L. and Zahniser, M.S.: Astigmatic mirror multipass absorption cells for long-path-length spectroscopy. Applied Optics, 34(18), 3336-3348, 1995.

Mihalopoulos, N., Barnes, I. and Becker, K. H.: Infrared absorption spectra and integrated band intensities for gaseous methanesulphonic acid (MSA), Atmos. Environ., 25(5), 807–812, 1992.

Novak, G. A., Fite, C. H., Holmes, C. D., Veres, P. R., Neuman, J. A., Faloona, I., Thornton, J. A., Wolfe, G. M., Vermeuel, M. P., Jernigan, C. M., Peischl, J., Ryerson, T. B., Thompson, C. R., Bourgeois, I., Warneke, C., Gkatzelis, G. I., Coggon, M. M., Sekimoto, K., Bui, T. P., Dean-Day, J., Diskin, G. S., DiGangi, J. P., Nowak, J. B., Moore, R. H., Wiggins, E. B., Winstead, E. L., Robinson, C., Thornhill, K. L., Sanchez, K. J., Hall, S. R., Ullmann, K., Dollner, M., Weinzierl, B., Blake, D. R. and Bertram, T. H.: Rapid cloud removal of dimethyl sulfide oxidation products limits SO_2 and cloud condensation nuclei production in the marine atmosphere, Proc. Natl. Acad. Sci., 118(42), e2110472118, doi:10.1073/PNAS.2110472118, 2021.

Patroescu, I. V., Barnes, I. and Becker, K. H.: FTIR kinetic and mechanistic study of the atmospheric chemistry of methyl thiolformate, J. Phys. Chem., 100(43), 17207–17217, doi:10.1021/jp961452u, 1996.

Rap, A., Scott, C. E., Spracklen, D. V., Bellouin, N., Forster, P. M., Carslaw, K. S., Schmidt, A. and Mann, G.: Natural aerosol direct and indirect radiative effects, Geophys. Res. Lett., 40(12), 3297–3301, doi:10.1002/grl.50441, 2013.

Saunders, S. M., Jenkin, M. E., Derwent, R. G. and Pilling, M. J.: Protocol for the development of the Master Chemical Mechanism, MCM v3 (Part A): Tropospheric degradation of non-aromatic volatile organic compounds, Atmos. Chem. Phys., 3(1), 161–180, doi:10.5194/acp-3-161-2003, 2003.

Veres, P. R., Andrew Neuman, J., Bertram, T. H., Assaf, E., Wolfe, G. M., Williamson, C. J., Weinzierl, B., Tilmes, S., Thompson, C. R., Thames, A. B., Schroder, J. C., Saiz-Lopez, A., Rollins, A. W., Roberts, J. M., Price, D., Peischl, J., Nault, B. A., Møller, K. H., Miller, D. O., Meinardi, S., Li, Q., Lamarque, J. F., Kupc, A., Kjaergaard, H. G., Kinnison, D., Jimenez, J. L., Jernigan, C. M., Hornbrook, R. S., Hills, A., Dollner, M., Day, D. A., Cuevas, C. A., Campuzano-Jost, P., Burkholder, J., Paul Bui, T., Brune, W. H., Brown, S. S., Brock, C. A., Bourgeois, I., Blake, D. R., Apel, E. C. and Ryerson, T. B.: Global airborne sampling reveals a previously unobserved dimethyl sulfide oxidation mechanism in the marine atmosphere, Proc. Natl. Acad. Sci. U. S. A., 117(9), 4505–4510, doi:10.1073/pnas.1919344117, 2020.

Wallace, J. M. and Hobbs, P. V.: Atmospheric science: an introductory survey, U. K. Elsevier Inc., 2006.

Wolfe, G. M., Marvin, M. R., Roberts, S. J., Travis, K. R. and Liao, J.: The framework for 0-D atmospheric modeling (F0AM) v3.1, Geosci. Model Dev., 9(9), 3309–3319, doi:10.5194/gmd-9-3309-2016, 2016.

Wu, R., Wang, S. and Wang, L.: New mechanism for the atmospheric oxidation of dimethyl sulfide. The importance of intramolecular hydrogen shift in a CH_3SCH_2OO radical, J. Phys. Chem. A, 119(1), 112–117, doi:10.1021/jp511616j, 2015.

Xu, L., Møller, K. H., Crounse, J. D., Otkjær, R. V., Kjaergaard, H. G. and Wennberg, P. O.: Unimolecular reactions of peroxy radicals formed in the oxidation of α-Pinene and β-Pinene by hydroxyl radicals, J. Phys. Chem. A, 123(8), 1661–1674, doi:10.1021/acs.jpca.8b11726, 2019.

Ye, Q., Goss, M. B., Isaacman-Vanwertz, G., Zaytsev, A., Massoli, P., Lim, C., Croteau, P., Canagaratna, M., Knopf, D. A., Keutsch, F. N., Heald, C. L. and Kroll, J. H.: Organic Sulfur Products and Peroxy Radical Isomerization in the OH Oxidation of Dimethyl Sulfide, ACS Earth Sp. Chem., 5(8), 2013–2020, doi:10.1021/acsearthspacechem.1c00108, 2021.

Yin, F., Grosjean, D. and Seinfeld, J. H.: Photooxidation of Dimethyl Sulfide and Dimethyl Disulfide. I: Mechanism Development, J. Atmos. Chem., (11), 309–365, 1990.

Zaytsev, A., Breitenlechner, M., Koss, A. R., Lim, C. Y., Rowe, J. C., Kroll, J. H. and Keutsch, F. N.: Using collision-induced dissociation to constrain sensitivity of ammonia chemical ionization mass spectrometry (NH_4^+ CIMS) to oxygenated volatile organic compounds, Atmos. Meas. Tech., 12(3), 1861–1870, doi:10.5194/amt-12-1861-2019, 2019.

https://doi.org/10.5194/acp-2022-566
Preprint. Discussion started: 15 August 2022

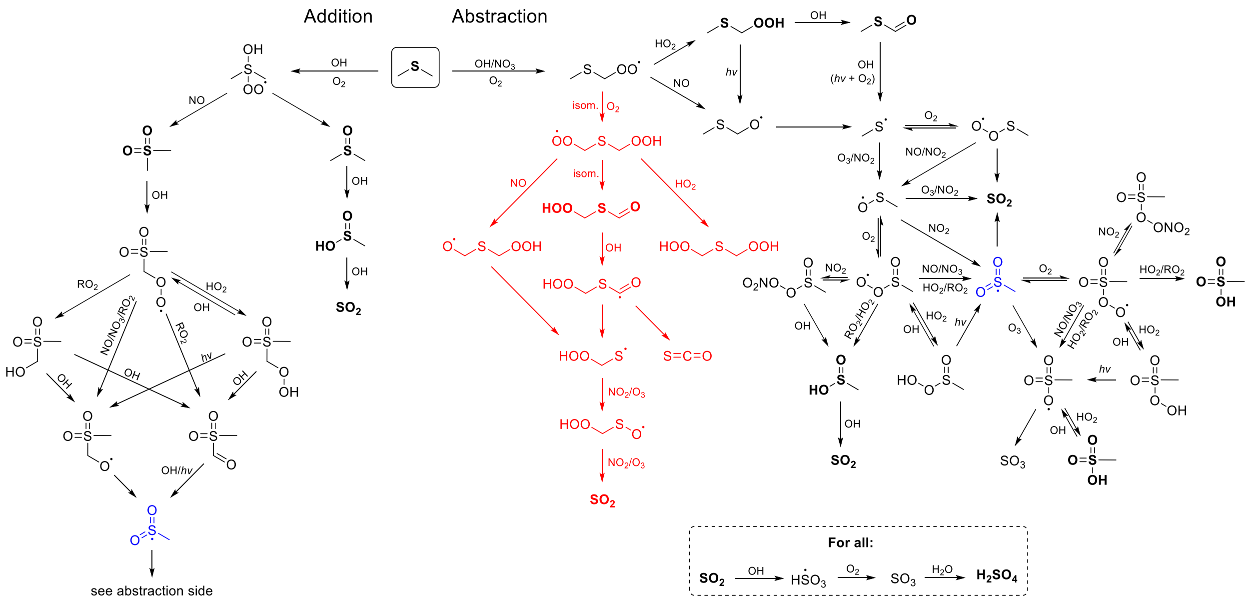

Figure 1: Gas-phase DMS+OH oxidation mechanism. Reactions in black are taken from MCM; reactions in red, related to hydroperoxymethyl thioformate (HPMTF, $HOOCH_2SCHO$) chemistry, are taken from Wu *et al* (Wu et al., 2015). Measured closed-shell compounds are shown in bold. Products that do not contain sulfur are not shown. The CH_3SO_2 radical (marked in blue) represents a link between addition and abstraction pathway products. Note that several products are shown multiple times.

Table 1: Summary of experimental conditions

Exp. No.	Precursor(s)[a]	OH precursor	$[OH]_{avg}$ (molec cm^{-3})	Dominant RO_2 fate	τ_{bi} (s)[b]	Seed particles	RH	Corresponding Figure(s)
1	~ 70 ppb DMS-$^{12}C_2$	HONO	~ 1×10^7	RO_2 + NO	< 0.1	NH_4NO_3	dry, <5%	Figure 2a, S4
2a[c]	~ 40 ppb DMS-$^{12}C_2$, ~ 40 ppb DMS-$^{13}C_2$	H_2O_2	~ 1.5×10^6	RO_2 isom.	> 10	NH_4NO_3	dry, <5%	Figure 2b, S5
2b[c]		NO and H_2O_2	~ 4×10^6	RO_2 + NO	< 0.1	NH_4NO_3	dry, <5%	Figure S5

3[d]	~ 35 ppb DMS-$^{12}C_2$, ~ 35 ppb DMS-$^{13}C_2$	H_2O_2 and HONO	~ 5 × 10^6	RO_2 isom. RO_2 + NO	< 0.1 – 10	NH_4NO_3	dry, <5%	Figure 3a, S8, S10
4	~ 70 ppb DMS-$^{12}C_2$	HONO	~ 1 × 10^7	RO_2 + NO	< 0.1	NaCl[e]	65 ± 3%	Figure 4, S11a
5	~ 40 ppb DMS-$^{12}C_2$, ~ 40 ppb DMS-$^{13}C_2$	H_2O_2 and HONO	~ 6 × 10^6	RO_2 isom.	> 1	$NaNO_3$	65 ± 3%	Figure 4, S11b

[a] To better separate HPMTF from N_2O_5, DMS-$^{13}C_2$ was used in low-NO experiments.
[b] Bimolecular lifetime of the CH_3SCH_2OO radical, calculated as $\tau_{bi} = (k_{RO2+HO2}[HO_2]+k_{RO2+NO}[NO])^{-1}$.
[c] Experiments 2a and 2b were carried out as part of a single oxidation experiment; initially (Exp. 2a) OH was generated from H_2O_2 photolysis (low-NO), then (Exp. 2b) 70 ppb of NO was injected into the chamber.
[d] ^{13}C Data in Experiment 3 were used to calculate k_{isom}; HONO was added multiple times in the experiment.
[e] The vaporizer in the AMS was operated at 800 °C. AMS calibration was done separately for 800°C.

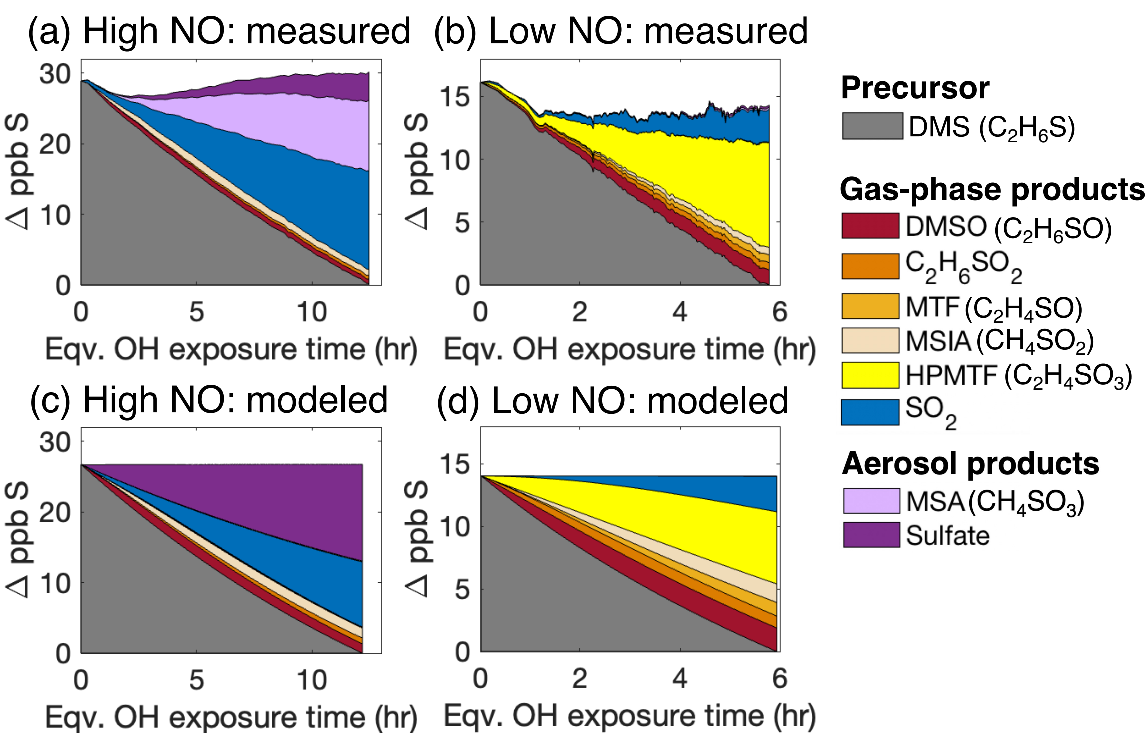

Figure 2: Stacked plots showing the total sulfur measured (a and b) and modeled (c and d) under high-NO (a and c) and low-NO (b and d) conditions. Data shown in (b) are from DMS-$^{12}C_2$ and DMS-$^{13}C_2$ combined. Products with a formula of $C_2H_6SO_2$ may be

https://doi.org/10.5194/acp-2022-566
Preprint. Discussion started: 15 August 2022

DMSO$_2$ and/or CH$_3$SCH$_2$OOH; under high-NO conditions, they are likely to be predominantly DMSO$_2$. Minor products detected but not listed in the legend due to their extremely low concentrations include CH$_2$SO$_2$ (a sulfene or thioacid) and CH$_3$SO$_6$N (likely methanesulfonyl peroxynitrate).

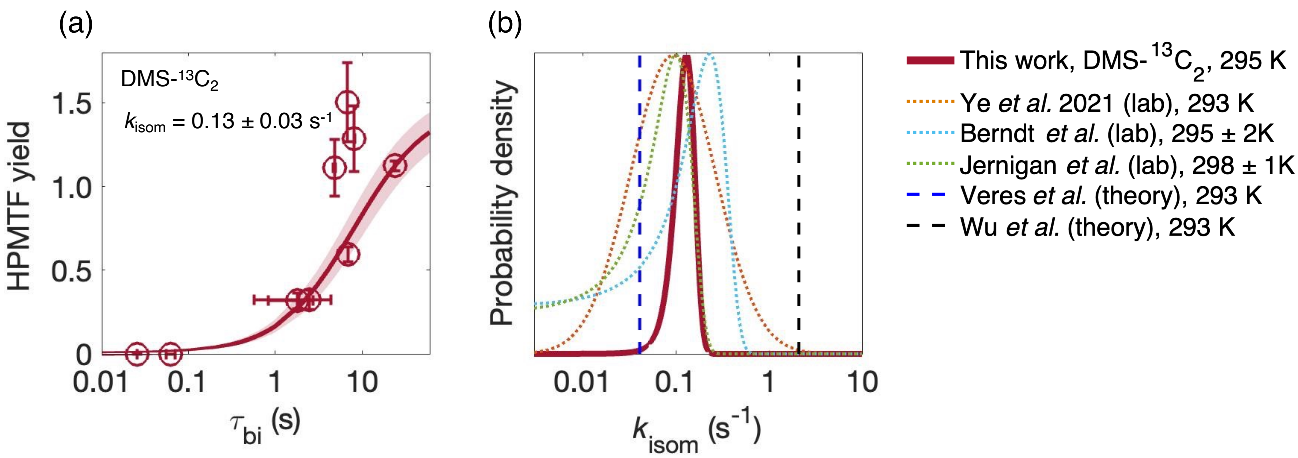

Figure 3: (a) The yield of HPMTF in the abstraction channel as function of the bimolecular lifetime τ_{bi} of CH$_3$SCH$_2$OO from the DMS-^{13}C$_2$ data. The shaded area is 1σ of the fit, which takes into account uncertainty in both τ_{bi} (arising from errors in [NO] and [HO$_2$]) on the x axis, and instrument noise on the y axis. Uncertainty in the CIMS sensitivity to HPMTF affects the absolute measurements but not the inflection point of the curve, or the derived value of k_{isom}. (b) Comparison of k_{isom} from this work with previous determinations of k_{isom} at 293-298 K (Berndt et al., 2019; Jernigan et al., 2022; Veres et al., 2020; Wu et al., 2015; Ye et al., 2021).

https://doi.org/10.5194/acp-2022-566
Preprint. Discussion started: 15 August 2022

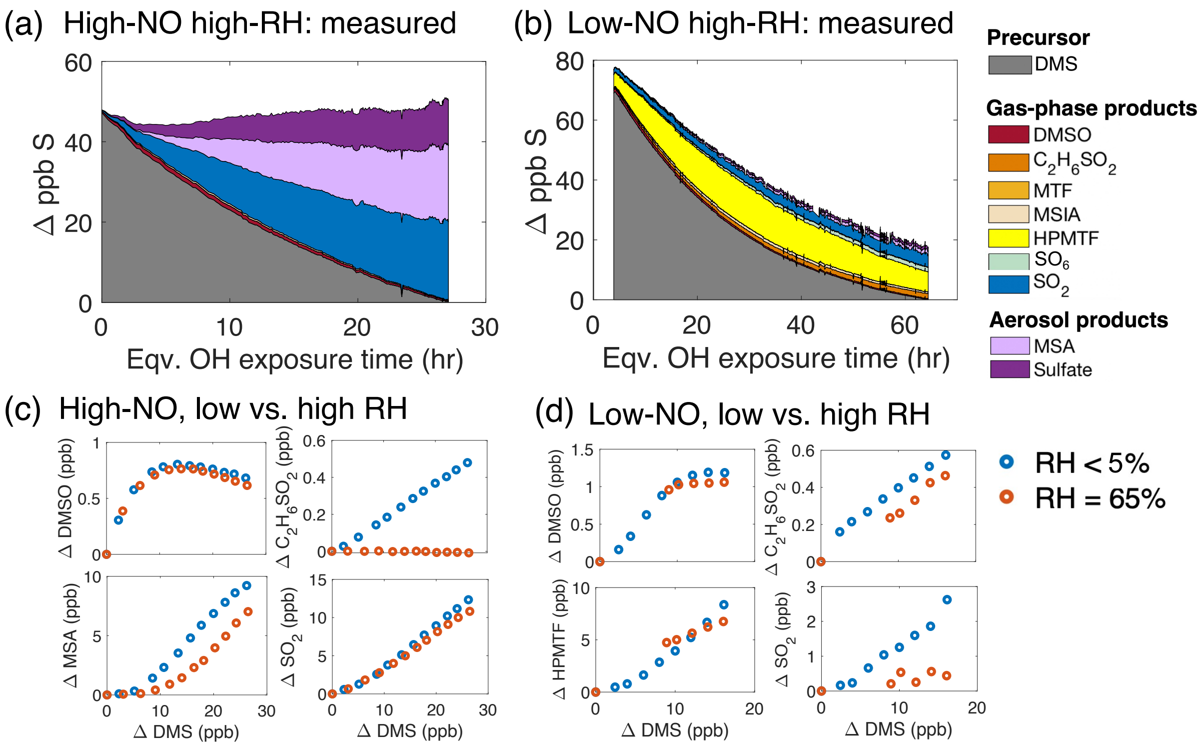

Figure 4: Results from the high-humidity (65% RH) DMS oxidation experiments. (a) Product formation under high-NO conditions (Exp. 4). (b) Product formation under low-NO conditions (Exp. 5). Because of instrument downtime, no data were collected for the first four hours of equivalent OH exposure. (c) Comparison of major species between the low-RH (Exp. 1) and high-RH experiment (Exp. 4) under high-NO condition. (d) Comparison of major species between the low-RH (Exp. 2) and high-RH experiment (Exp. 5) under low-NO conditions. Change in product concentration is plotted against change in DMS concentration over the initial 6 hrs of OH exposure.